Adaptive Network Automata Modelling of Complex Networks for Link Prediction

Jialin Zhao , Alessandro Muscoloni , Umberto Michieli , Yingtao Zhang , Carlo Vittorio Cannistraci *

Posted Date: 28 May 2025

doi: 10.20944/preprints202012.0808.v4

Keywords: complex networks; network models; link prediction; automata theory; network automata; Cannistraci-Hebb theory

 doi:10.20944/preprints202012.0808.v4

Article

Adaptive Network Automata Modelling of Complex Networks for Link Prediction

Jialin Zhao [1,2], Alessandro Muscoloni [1,3], Umberto Michieli [4], Yingtao Zhang [1,2] and Carlo Vittorio Cannistraci [1,2,3]

[1] Center for Complex Network Intelligence (CCNI), Research Center in Tsinghua Laboratory of Brain and Intelligence (THBI), Department of Psychological and Cognitive Sciences; jialin.zhao97@gmail.com (J.Z.); alessandro.muscoloni@gmail.com (A.M.); zhangyingtao1024@gmail.com (Y.Z.)
[2] Dept. of Computer Science, Tsinghua University, China
[3] Dept. of Biomedical Engineering, Tsinghua University, China
[4] University of Padova, Italy; umberto.michieli1@gmail.com
* Correspondence: kalokagathos.agon@gmail.com

Abstract: Many complex networks have a connectivity that might be only partially detected or that tends to grow over time, hence the prediction of non-observed links is a fundamental problem in network science. The aim of topological link prediction is to forecast these non-observed links by only exploiting features intrinsic to the network topology. It has a wide range of real applications, like suggesting friendships in social networks or predicting interactions in biological networks. The Cannistraci-Hebb theory is a recent achievement in network science that includes a theoretical framework to understand local-based link prediction on paths of length n. In this study we introduce two innovations: one on the theory of modelling (science) and the other on the theory of realization (engineering). For the theory of modelling we first recall a definition of network automata as a general framework for modelling the growth of connectivity in complex networks. We then show that several deterministic models previously developed fall within this framework and we introduce novel network automata following the Cannistraci-Hebb rule. For the theory of realization, we present how to build adaptive network automaton for link prediction, which incorporate multiple deterministic models of self-organization and automatically learns the rule that better explains the patterns of connectivity in the network under investigation. We compare the Cannistraci-Hebb Adaptive (CHA) network automaton against state-of-the-art link prediction methods, including structural perturbation method (SPM), stochastic block models (SBM), and artificial intelligence algorithms for graph representation learning, such as graph embedding methods and message-passing-based models. In particular, we compare the Message Passing Link Predictor (MPLP), a state-of-the-art link prediction method that differs from general-purpose graph embedding methods by approximating heuristic scores such as Common Neighbor through quasi-orthogonal message-passing. We also compare with MPLP+, a scalable variant that avoids costly preprocessing by leveraging only one-hop neighborhoods. CHA displays an overall higher link prediction performance across different evaluation frameworks on 1269 networks across 14 complex systems domains. Finally, we highlight that CHA offers the key advantage to explicitly explain the mechanistic rule of self-organization which leads to the link prediction performance, whereas SPM, SBM, and AI-based methods like graph embeddings and MPLP do not. In comparison to CHA, SBM unfortunately shows irrelevant and unsatisfactory performance demonstrating that SBM modelling is not adequate for link prediction in real networks.

Keywords: complex networks; network models; link prediction; automata theory; network automata; Cannistraci-Hebb theory

1. Introduction

Many complex networks have a connectivity that might be only partially detected or that tends to grow over time, hence the prediction of non-observed links is a fundamental problem in network

 doi:10.20944/preprints202012.0808.v4

science. The aim of topological link prediction is to forecast these non-observed links by only exploiting features intrinsic to the network topology. It has a wide range of real applications, like suggesting friendships in social networks or predicting interactions in biological networks [1–3]. A plethora of methods based on different methodological principles have been developed in recent years, and in this study we will consider for reference the state-of-the-art algorithms. The first is Structural Perturbation Method (SPM), a model-free global approach that relies on a theory derived from the first-order perturbation in quantum mechanics [4]. The second represents a class of generative models named Stochastic Block Models (SBM), whose general idea is that the nodes are partitioned into groups and the probability that two nodes are connected depends on the groups to which they belong [5]. The third class of methods is model-free and includes machine learning algorithms for graph embedding. Such methods convert the graph data into a low dimensional space in which certain graph structural information and properties are preserved. Different graph embedding variants have been developed aiming to preserve different information in the embedded space, some examples are: HOPE [6], node2vec [7], NetSMF [8], ProNE [9]. A fourth class of methods includes message-passing neural networks specifically designed for link prediction. Among them, the Message Passing Link Predictor (MPLP) [10] approximates structural heuristics such as Common Neighbor by leveraging quasi-orthogonal vector propagation within a pure message-passing framework.

While the aforementioned approaches have been shown to be competitive link predictors, they do not offer a clear interpretability of the mechanisms behind the network growth. This property, instead, can be fulfilled for example by mechanistic models based on the Cannistraci-Hebb theory [3,11–15], since each of them is based on an explicit deterministic mathematical formulation. Each model in the Cannistraci-Hebb theory represents a specific rule of self-organization which is associated to explicit principles that drive the growth's dynamics of the underlying complex networked physical system.

The Cannistraci-Hebb theory is a recent achievement in network science [15,16] that includes a theoretical framework to understand local-based link prediction on paths of length n. It includes any type of classical local link predictor based on paths of length two such as common neighbors (CN) [17], resource allocation (RA) [18], Jaccard [19] and preferential attachment (PA) [17]; and link predictor on paths of length three of Kovács et al. [20], which triggered a fundamental discovery on the organization of protein interaction networks (PPI). Following the discovery of a previous article of Daminelli et al. [11] that stressed the importance of paths of length three for link prediction in bipartite networks, on the same line Kovács et al. suggested that proteins interact according to an underlying bipartite scheme. Indeed, proteins interact not if they are similar to each other, but if one of them is similar to the other's partners. This principle, such as the one proposed by Daminelli et al. [11], mathematically relies on network paths of length three (L3) [20], whereas most of the deterministic local based models previously developed were based on paths of length two (L2) [3]. These findings lead to a change of perspective in the field, highlighting the existence of different classes of networks whose patterns of interactions are organized either as L2 or L3. However, a conceptual limitation of the studies of Daminelli et al. [11] and Kovács et al. is that the L3-based link predictors developed [20] were not properly connected to already known principles of modelling, which prompted us to formulate and introduce a generalized theory.

In this study, we introduce four key innovations in the field of topological link prediction:

- **Minimization of external connectivity (CH paradigm).** We formalize a new principle within the Cannistraci-Hebb (CH) framework that emphasizes minimizing external local-community links (eLCL), leading to the introduction of two new models, CH3 and CH3.1.
- **Adaptive model selection.** We design an adaptive mechanism that automatically selects the most suitable CH model and path length for each network, based on internal validation performance. This removes the need for manual tuning and ensures better alignment with the network's structural features. Empirically, on a benchmark of over 1000 networks, our adaptive method achieves more than **twice the win rate** of the best-performing baseline.

 doi:10.20944/preprints202012.0808.v4

- **Comprehensive static and temporal benchmark.** We construct a large-scale benchmark ATLAS, consisting 1269 real-world networks (ATLAS-static) and 14 time-evolving networks (ATLAS-temporal).
- **Multi-metric evaluation.** We adopt three complementary evaluation metrics, Precision, NDCG, and AUPR, to capture diverse aspects of link prediction performance. Across all three metrics, our adaptive model **consistently outperforms** all baselines, demonstrating its robustness and general superiority under different evaluation criteria.

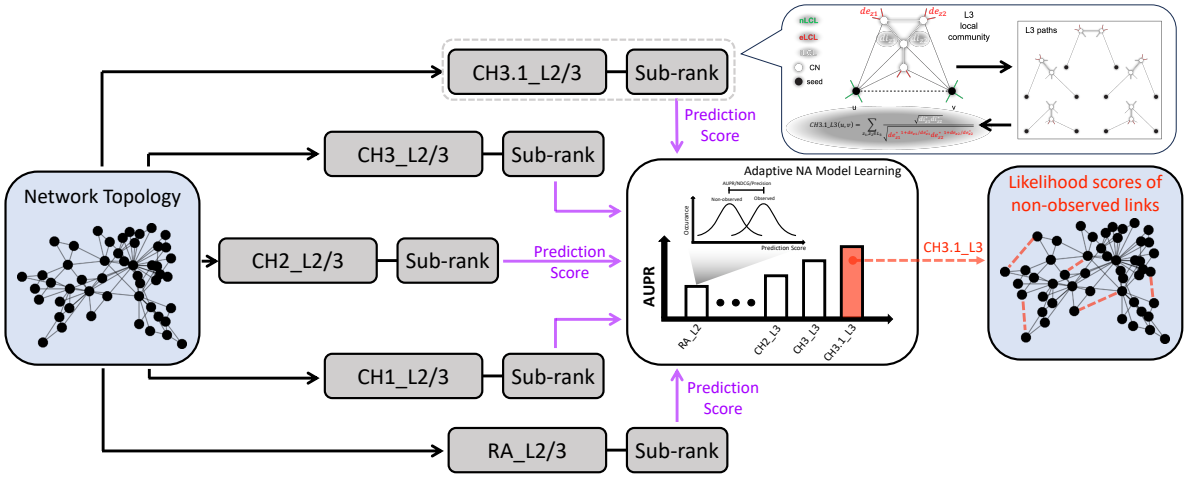

Figure 1. Illustration of the Cannistraci-Hebb Adaptive (CHA) network automaton framework. CHA is designed to automatically adapt to the structural characteristics of the input network by selecting the most suitable Cannistraci-Hebb (CH) model and path length for link prediction. For a given network, multiple CH models (e.g., CH2, CH3) and path lengths (e.g., *L*2, *L*3) are applied independently to assign likelihood scores to both observed and non-observed links. For each model-path combination, a performance metric, such as Area Under the Precision-Recall Curve (AUPR), Precision, or NDCG, is computed using observed links as positives. The combination achieving the highest value under the selected metric is chosen, and the corresponding scores for the non-observed links are used as the final prediction. To further refine the ranking among node pairs receiving identical CH scores, a sub-ranking strategy based on Spearman correlation of shortest-path profiles is applied. This adaptive procedure ensures that CHA selects the rule best aligned with the underlying connectivity pattern of the network under analysis.

2. Preliminaries and Methods

2.1. Science of Physical Modelling

2.1.1. Network Automata

CH and CHA are network automata rules for approximating the likelihood of a non-observed link to appear in the network. These rules are categorized as network automata because they adopt only local information to infer the score of a link in the network without need of pre-training of the rule. Note that CH and CHA are predictive network automata that differ from generative network automata which are rules created to generate artificial networks [21–23]. The concept of *network automata* was originally introduced by Wolfram [24] and later formally defined by Smith et al. [25] as a general framework for modeling the evolution of network topology. Given an unweighted and undirected adjacency matrix $X(t)$ at time t, in a network automaton the states of links evolve over time according to a rule that depends only on local topological properties computable from a portion of the adjacency matrix $\tilde{X}(t) \subset X(t)$:

$$\tilde{X}(t+1) = F(\tilde{X}(t)) \tag{1}$$

The ruleset may depend on any property of the nodes or links and might be deterministic or stochastic. In contrast to cellular automata on a network [24,26], in which the states of nodes evolve and whose neighborhoods are defined by the network, in network automata the states of links evolve, and therefore the topology itself changes over time.

 doi:10.20944/preprints202012.0808.v4

Smith et al. [25] provide an example in which the state update of a link $X_{u,v}(t+1)$ is determined by a simple topological property such as the sum of the node degrees:

$$f_{u,v}(t) = d_u(t) + d_v(t) \tag{2}$$

If the link exists, $X_{u,v}(t) = 1$, and the property exceeds a survival threshold $f_{u,v}(t) > x_S$, then the link survives; otherwise, it is removed. If the link does not exist, $X_{u,v}(t) = 0$, and the property exceeds a birth threshold $f_{u,v}(t) > x_B$, then the link is created; otherwise, it remains absent. In this example, the computation of the topological property and the link update based on the survival and birth thresholds constitute the F operation. This basic ruleset fully describes the evolution of a network automaton.

We note that if we focus on the topological property $f_{u,v}(t)$, we could replace the sum of node degrees with any of several mathematical models developed for link prediction, such as common neighbors (CN) [17], resource allocation (RA) [18], Jaccard [19], and preferential attachment (PA) [17]. Although these models are often referred to as heuristics, the definition and example above clearly show that such local and deterministic models are in fact network automata.

As a final remark, in this link prediction study we specifically use these algorithms to predict the non-observed links that are more likely to be created at the next step of network evolution. Therefore, we do not consider the survival and birth thresholds in further detail, and focus solely on the topological property $f_{u,v}(t)$. For simplicity, we will also omit the time variable t in the following discussion.

2.1.2. Network Automata on Paths of Length n

After having recalled the framework of network automata defined by Smith et al. [25], we now introduce a particular subclass named *network automata on paths of length n*. These automata evaluate the topological property between two nodes based on the topological information contained along the paths of length n between them. In mathematical terms, we can express the topological property as follows:

$$f(u,v) = \sum_{z_1,\ldots,z_{n-1} \in L_n} f'(z_1,\ldots,z_{n-1}) \tag{3}$$

where u and v are the two seed nodes of the candidate interaction; the summation is executed over all paths of length n; $z_1,\ldots,z_{n-1}$ are the intermediate nodes on each path of length n; and $f'(z_1,\ldots,z_{n-1})$ is some function dependent on the intermediate nodes.

A simple example is represented by the *resource allocation* (RA) model developed by Zhou et al. [18], which is a network automaton on paths of length two ($L2$), using as function $f'(z)$ the inverse of the degree of the intermediate node (common neighbour in the $L2$ case). The mathematical formula is:

$$\text{RA-L2}(u,v) = \sum_{z \in L_2} \frac{1}{d_z} \tag{4}$$

where the summation is over all paths of length two; z is the intermediate node on each path; and d_z is the degree of node z.

To generalize this to paths of length $n > 2$, we need an operator that merges the individual topological contributions of the intermediate nodes on a path of length n. Without loss of generality, if we use the geometric mean as the merging operator, we derive the following generalized formula for RA on paths of length n:

$$\text{RA-Ln}(u,v) = \sum_{z_1,\ldots,z_{n-1} \in L_n} \frac{1}{\left(d_{z_1} d_{z_2} \cdots d_{z_{n-1}}\right)^{\frac{1}{n-1}}} \tag{5}$$

where the summation is executed over all paths of length n; $z_1,\ldots,z_{n-1}$ are the intermediate nodes; and $d_{z_1},\ldots,d_{z_{n-1}}$ are their respective degrees.

We note that for paths of length three ($L3$), the above formula becomes equivalent to the one proposed by Kovács et al. [20], which extends the resource allocation principle to paths of length

 doi:10.20944/preprints202012.0808.v4

three—although this connection was not properly clarified in their study, but was subsequently explained in [15] supporting the present one. From here onward, we will refer to this method as *RA-L3*.

2.1.3. Cannistraci-Hebb Network Automata on Paths of Length n

In this section, we introduce a new rule of self-organization that can be modeled using different network automata on paths of length n. Let us first recall some theoretical background.

In 1949, Donald Olding Hebb proposed a local learning rule in neuronal networks, often summarized as: *neurons that fire together wire together* [27]. However, the concept of "wiring together" was not fully specified and can be interpreted in two ways. The first interpretation is that existing connectivity between co-firing neurons is reinforced. The second is that new connections form between co-firing neurons not yet directly connected but already integrated within the same interacting cohort.

In 2013, Cannistraci et al. [3] termed the second interpretation *epitopological learning*, noting that it could be formalized as a topological link prediction problem in complex networks. The rationale is that, in networks with local-community organization, cohorts of neurons tend to be co-activated (fire together) and to learn by forming new connections (wire together), because they are topologically isolated within the same local community.

Cannistraci et al. [3] postulated that epitopological learning in neuronal networks is a special case of a more general rule of local learning, valid for topological link prediction in any complex network exhibiting a *local-community-paradigm* (LCP) architecture. Based on this idea, they introduced a new class of link predictors which outperformed state-of-the-art predictors in both monopartite [3,28–34] and bipartite topologies [11,12], across various domains such as brain networks, social networks, biological systems, and economic structures.

A study by Narula et al. [35] also highlighted that LCP and epitopological learning enhance the understanding of local brain connectivity in processing, learning, and memorizing chronic pain.

Previous formulations of the LCP theory emphasized the contribution of common neighbor nodes complemented by the interactions among them, termed internal local-community links (iLCL). This was a limitation, as shown by Cannistraci [13], who demonstrated that the local isolation of common neighbors, minimizing their interactions external to the local community (external local-community links, eLCL), is equally important to carve the LCP architecture. This minimization forms a topological energy barrier that confines information processing within the community.

Here, we introduce the **Cannistraci-Hebb (CH)** rule, a revised mathematical formalization of the LCP theory. It represents any rule that explicitly incorporates the minimization of eLCL, which is the **necessary** condition for being a CH rule. We define *Cannistraci-Hebb network automata on paths of length* n as any network automaton in which the function $f'(z_1, \ldots, z_{n-1})$ follows the CH rule.

The first CH model, introduced by Cannistraci et al. [3] and originally named *Cannistraci-Resource-Allocation (CRA)*, is renamed here as CH1. Its formula for $L2$ is:

$$\text{CH1-L2}(u,v) = \sum_{z \in L_2} \frac{di_z}{d_z} \tag{6}$$

where di_z is the internal degree (number of iLCL) of the intermediate node z, and $d_z = 2 + \text{iLCL} + \text{eLCL}$ is the total degree. This model encourages minimization of eLCL, but only when $d_z^{\text{int}} > 0$, otherwise the node does not contribute to the sum.

To address this, Cannistraci et al. [15] proposed the second CH model:

$$\text{CH2-L2}(u,v) = \sum_{z \in L_2} \frac{1 + di_z}{1 + de_z} \tag{7}$$

where di_z and de_z are the internal and external degrees (iLCL and eLCL) of node z, respectively. The unitary terms in the numerator and denominator prevent saturation when either value is zero.

 doi:10.20944/preprints202012.0808.v4

Next, we introduce **CH3**, a novel model proposed for the first time in this study, which mathematically represents the basic principle of being a CH rule. Indeed, CH3 is based solely on eLCL minimization:

$$\text{CH3-L2}(u,v) = \sum_{z \in L_2} \frac{1}{1+de_z} \tag{8}$$

CH3 departs from earlier formulations by fully discarding the internal degree component and focusing purely on penalizing external connectivity, providing a clean and principled expression of the CH paradigm.

Finally, we propose **CH3.1**, which embodies an adaptive mechanism: it accounts for the reward of internal links di_z when the node z follows the CH principle (because its number of external links de_z is low), and progressively neglects the reward di_z for larger values of external links de_z, which indicates a violation of the CH principle:

$$\text{CH3.1-L2}(u,v) = \sum_{z \in L_2} \frac{1+di_z}{(1+de_z)^{1+\frac{de_z}{1+de_z}}} \tag{9}$$

We note that the RA model is also a CH network automaton, while CN is not. In this study, we focus on five CH models: RA, CH1, CH2, CH3 and CH3.1. We do not consider non-CH models, including those studied by Kovács et al. [20], as they were shown to underperform.

Similar to RA, the CH models can be generalized to paths of length n (L_n). Their formulas for $L2$, $L3$, and Ln are summarized in Figure A1. In the generalized case, the local community is the set of all intermediate nodes in any path of length n between the seed nodes. iLCL are the internal links among those nodes; eLCL are the links between any intermediate node and external nodes (excluding the seed nodes).

2.1.4. CH Model Sub-Ranking Strategy

Here we describe the sub-ranking strategy adopted by the CH model to internally sub-rank all node pairs that receive the same CH score. The goal is to refine link prediction by reducing the ranking uncertainty among node pairs that are tied-ranked.

Given a network and a set of CH scores $\text{CH}_{i,j}$ computed for all node pairs (i,j) according to a given CH model, the sub-ranking procedure proceeds as follows:

1. Assign to each link (i,j) in the network a weight $w_{i,j} = \max_{k,l} \text{CH}_{k,l} + \min_{k,l} \text{CH}_{k,l} - \text{CH}_{i,j}$ to transform similarity into dissimilarity.
2. Compute the shortest paths (SP) between all node pairs in the resulting weighted network.
3. For each node pair (i,j), compute the prediction score $\text{SPcorr}_{i,j}$ as the Spearman's rank correlation between the two vectors of all shortest paths from node i and from node j to every other node in the network.
4. Generate a final ranking of node pairs such that pairs are first ranked by $\text{CH}_{i,j}$, and any ties are sub-ranked using $\text{SPcorr}_{i,j}$. If both scores are tied, then the node pairs receive the same final rank.
5. (Optional) Map the final ranking back to a likelihood score if a numerical prediction score is required by downstream applications (see details in Appendix G).

Although the SPcorr score could be replaced by other link predictors, we chose this approach for its neurobiological grounding, which aligns with the CH model's conceptual framework. Specifically, based on one interpretation of *Peters' rule*, the probability of two neurons being connected is proportional to the spatial apposition of their respective axonal and dendritic arbors [36]. In other words, connectivity depends on the geometrical proximity of neurons.

This biological principle resonates with the SPcorr score within the CH modelling framework: a high correlation implies that two nodes share similar shortest-path distances to all other nodes, which suggests, within the network topology, that they are spatially proximate due to their network-geometric closeness.

 doi:10.20944/preprints202012.0808.v4

2.2. Engineering the Adaptive Network Automata Machine

Different types of complex networks exhibit distinct structural patterns, some are better captured by $L2$ connectivity, others by $L3$, making it unlikely that a single network automaton rule can perform optimally across all domains (see Figure A2). For instance, $L2$-based rules may suit social networks, whereas protein–protein interaction (PPI) networks often favor $L3$-based approaches.

Here, we aim to go a step further from the engineering perspective and design a computational machine that is adaptive to the network under investigation and is capable of automatically selecting the model that is most likely to provide the best prediction.

To achieve this, we exploit a particular property of the network automata models discussed in Section 2.1. These deterministic rules for link prediction assign scores to both observed and non-observed links in a way that is directly comparable; that is, the scores of observed links are not inherently biased to be higher or lower than those of non-observed links. This is because the mathematical formulation used to compute the score between two nodes is independent of the existence of the link in the current topology.

Specifically, given a set of candidate models and a network, we compute a metric (e.g., AUPR, Precision, or NDCG) based on how well each model separates observed from non-observed links. The assumption is that, if the model tends to assign higher scores to observed links than to non-observed links, it is likely more effective at predicting missing or future links.

This mechanism enables CHA to self-adapt to a wide range of network topologies. The time complexity and runtime details are provided in Appendix F.

3. Experiments

3.1. Datasets and Baselines

3.1.1. Datasets

We evaluate our methods on a comprehensive collection of real-world networks drawn from two benchmark sets:

- **ATLAS-static** includes 1269 undirected static networks from 14 domains such as biological, social, and economic systems (see Appendix for full details).
- **ATLAS-temporal** consists of 14 real-world networks with temporal snapshots representing dynamic evolution across time (see Appendix for details).

For static networks, we adopt a 10% link removal evaluation protocol: 10% of existing edges are randomly removed from the original network and used as positives in a held-out test set, while the remaining links form the input to the prediction algorithm. The evaluation is repeated 10 times with different random splits, and the average metric is reported. For temporal networks, we evaluate predictions across successive snapshots: links that appear at future time steps are used as positives, while links absent at prediction time are ranked and scored. The average performance across all time pairs is reported. Full evaluation protocols are described in Appendix.

3.1.2. Baselines

We compare the proposed CHA framework against four categories of state-of-the-art link prediction methods:

- **SPM** (Structural Perturbation Method) [4]: a model-free global approach based on spectral perturbation.
- **SBM variants** [5,37,38]: including SBM, degree-corrected SBM, and nested extensions.
- **Graph Embedding Methods**: including HOPE [6], node2vec [7], NetSMF [8], and ProNE [9].
- **MPLP and MPLP+** [10]: message-passing models designed to approximate structural heuristics for link prediction.

 doi:10.20944/preprints202012.0808.v4

Detailed descriptions of all baseline methods, including their underlying principles, implementation details, and hyperparameter settings, as well as complete evaluation procedures, are provided in the Appendix.

3.1.3. Scale of Evaluation

Unlike prior work that typically evaluates on a limited number of networks (often fewer than 20), our study conducts large-scale benchmarking on a total of 1283 real-world networks (1269 static and 14 temporal). This represents the most extensive evaluation to date for the link prediction task. Table 1 summarizes the number of networks used in related literature, highlighting the comprehensiveness of our experimental setup.

Table 1. Number of real-world networks tested for the link prediction task in related literature.

Algorithm	Field	Year	Networks	Ref.
SBM	Statistical Physics	2014	8	[37]
SBM-DC	Statistical Physics	2014	5	[38]
SBM-N, SBM-DC-N	Statistical Physics	2014	33	[5]
SPM	Quantum Physics	2015	13	[4]
HOPE	Computer Science	2016	4	[6]
node2vec	Computer Science	2016	3	[7]
ProNE, ProNE-SMF	Computer Science	2019	5	[9]
NetSMF	Computer Science	2019	5	[8]
MPLP, MPLP+	Computer Science	2024	15	[10]
CHA	**Physics & CS**	**2025**	**1283**	**Ours**

3.2. Link Prediction on ATLAS-Static

To evaluate robustness across network scales, we define three nested subsets of the ATLAS-static dataset: **ATLAS-small** ($N \leq 100$, 900 networks), **ATLAS-medium** ($N \leq 2500$, 1126 networks), and **ATLAS-large** ($N \leq 10000$, 1269 networks). As shown in Figures 2, CHA consistently achieves both the highest win rate and the best average rank across all three settings, outperforming SPM, all SBM variants, graph embedding methods (HOPE, node2vec, NetSMF, ProNE), and message-passing models (MPLP and MPLP+). Notably, CHA achieves more than **twice the win rate** of other baselines under AUPR, underscoring the strength of its adaptive mechanism. These results highlight CHA's superiority not only in winning the top position more frequently but also in maintaining consistently strong performance across networks of varying size and structure.

 doi:10.20944/preprints202012.0808.v4

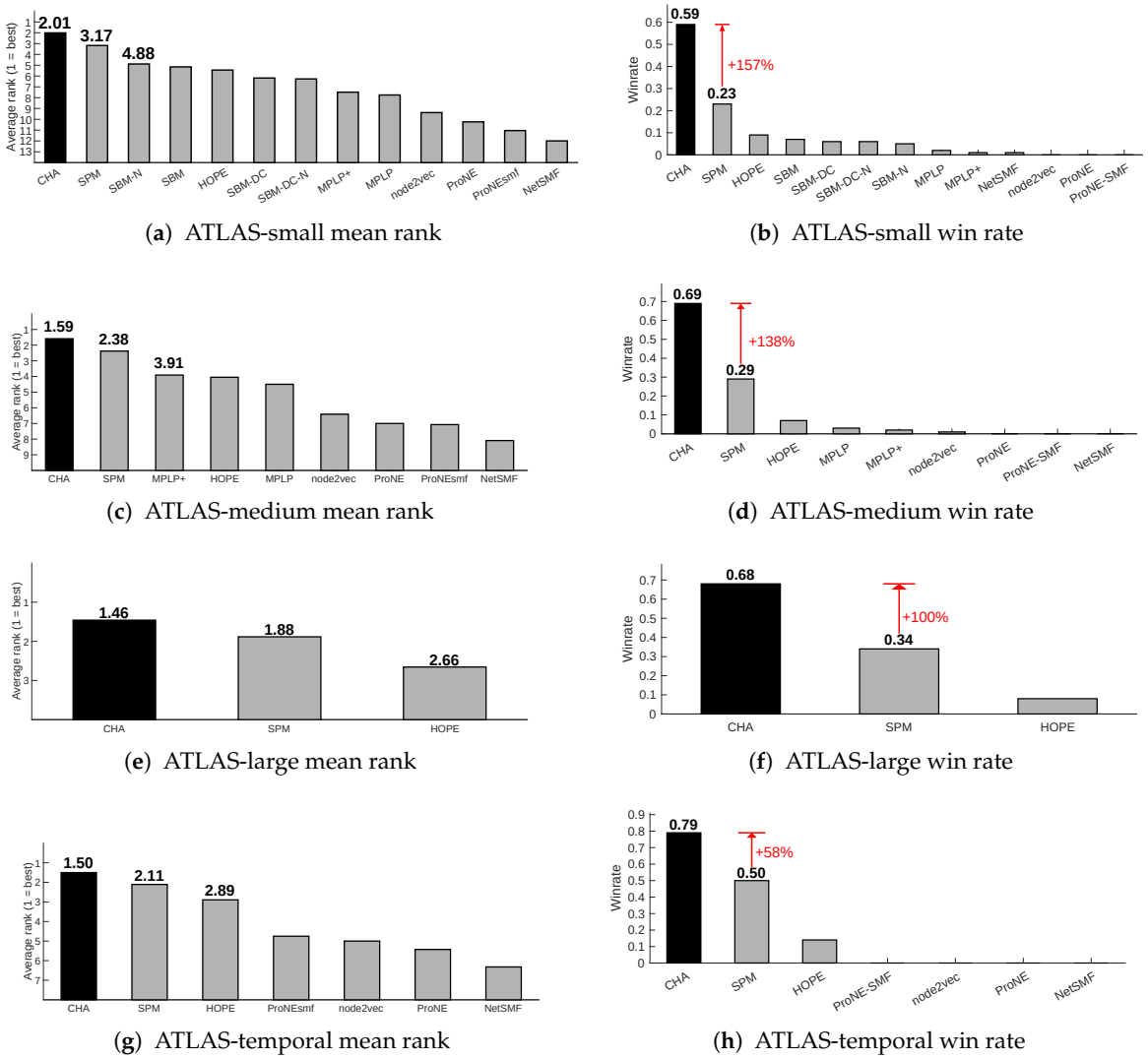

(**a**) ATLAS-small mean rank

(**b**) ATLAS-small win rate

(**c**) ATLAS-medium mean rank

(**d**) ATLAS-medium win rate

(**e**) ATLAS-large mean rank

(**f**) ATLAS-large win rate

(**g**) ATLAS-temporal mean rank

(**h**) ATLAS-temporal win rate

Figure 2. Comparison of CHA with baseline methods across network categories using AUPR. Each pair of subplots compares the performance of CHA and baselines in terms of **(left)** mean rank and **(right)** win rate across: **(a, b)** ATLAS-small ($N \leq 100$, 900 networks), **(c, d)** ATLAS-medium ($N \leq 2500$, 1126 networks), **(e, f)** ATLAS-large ($N \leq 10000$, 1269 networks), and **(g, h)** ATLAS-temporal (14 time-evolving networks). CHA consistently achieves the best mean rank and highest win rate across all categories.

Detailed performance breakdowns for each method across the 14 network classes in the ATLAS-static dataset are provided in supplementary material. Additional mean-rank and win-rate comparisons based on NDCG and Precision are also reported in Figures A3 and A4, confirming the consistency of CHA's superiority under multiple evaluation metrics.

3.3. Temporal Link Prediction

We further evaluate the generalization of CHA in time-evolving settings using 14 real-world temporal networks from the ATLAS-temporal collection. Figures 2g,h report the performance of CHA compared to baseline methods in terms of mean rank and win rate based on AUPR, respectively. CHA ranks among the top-performing methods and achieves the best mean rank and highest win rate. These results indicate that CHA is well-suited for modeling dynamic connectivity in temporal networks, offering stable and competitive predictions across diverse time-evolving settings.

 doi:10.20944/preprints202012.0808.v4

3.4. Path Length Preference Across Network Classes

To better understand the need for adaptivity in CHA, we analyze how different network classes prefer different path lengths. For each network in the ATLAS-static dataset ($N \leq 10000$), and for each CH model (RA, CH1, CH2, CH3, CH3.1), we apply the 10% link removal protocol and compute AUPR on both $L2$ and $L3$ paths. For each network and path length, we record the maximum AUPR across all CH models.

Figure A2 reports, for each network class, the win rate of $L2$ versus $L3$, i.e. how often one path length outperforms the other within the class. The results clearly show that no single path length dominates across all classes: some network types (e.g., coauthorship or connectome) are better captured by $L2$ structures, while others (e.g., PPI or transcription) favor $L3$.

This observation provides empirical motivation for using an adaptive mechanism that automatically selects the most suitable path length and CH model for each network, rather than relying on a fixed configuration. Similar trends are observed when using Precision and NDCG as evaluation metrics (see Appendix Figures A5 and A6).

3.5. Validation of the CH Adaptive Strategy

The CHA framework operates by adaptively selecting, for each network, the CH model and path length combination that achieves the best predictive performance on observed links. In this study, we instantiate CHA using the CH3 and CH3.1 models, as they best capture the core CH principle of minimizing external links (eLCL).

To directly assess the value of the adaptive mechanism in CHA, we compare its performance with all individual CH variants (RA, CH1, CH2, CH3, CH3.1) under the same 10% link removal evaluation on the full ATLAS-static dataset ($N \leq 10000$, 1269 networks). For each network, we identify the winning method per metric, and report the average win rate across the 14 network classes.

Figure A7 shows results under three metrics: AUPR, Precision, and NDCG. In all cases, CHA outperforms every individual CH variant, consistently achieving the highest win rate. This confirms the effectiveness of the adaptive design in CHA, which dynamically selects the best CH model and path length combination for each network rather than relying on a fixed configuration.

We also compare this choice against other combinations of CH models and report the win rate of each configuration on the ATLAS-static dataset. As shown in Table A1, the {CH3, CH3.1} setting achieves the highest win rate, confirming its effectiveness as the optimal rule set for CHA.

4. Conclusions and Discussion

We proposed **Cannistraci-Hebb Adaptive (CHA)**, a new network automata based on topological self-organization and the minimization of external connectivity. CHA leverages two models, CH3 and CH3.1, and adaptively selects the optimal path length per network to capture local community dynamics. Experiments on more than 1000 real networks, static and temporal, show that CHA consistently outperforms state-of-the-art baselines across multiple metrics. This confirms the effectiveness of combining theoretical grounding with adaptive selection.

While CHA is deterministic and interpretable, it does not leverage node attributes, which may be crucial in some domains. Future extensions could integrate topological and feature-based signals. CHA can support applications such as recommender systems or biological discovery, but its use on sensitive data should be carefully monitored to avoid unintended inferences.

Acknowledgments: This work was supported by the Zhou Yahui Chair Professorship award of Tsinghua University (to CVC), the National High-Level Talent Program of the Ministry of Science and Technology of China (grant number 20241710001, to CVC).

 doi:10.20944/preprints202012.0808.v4

Appendix A

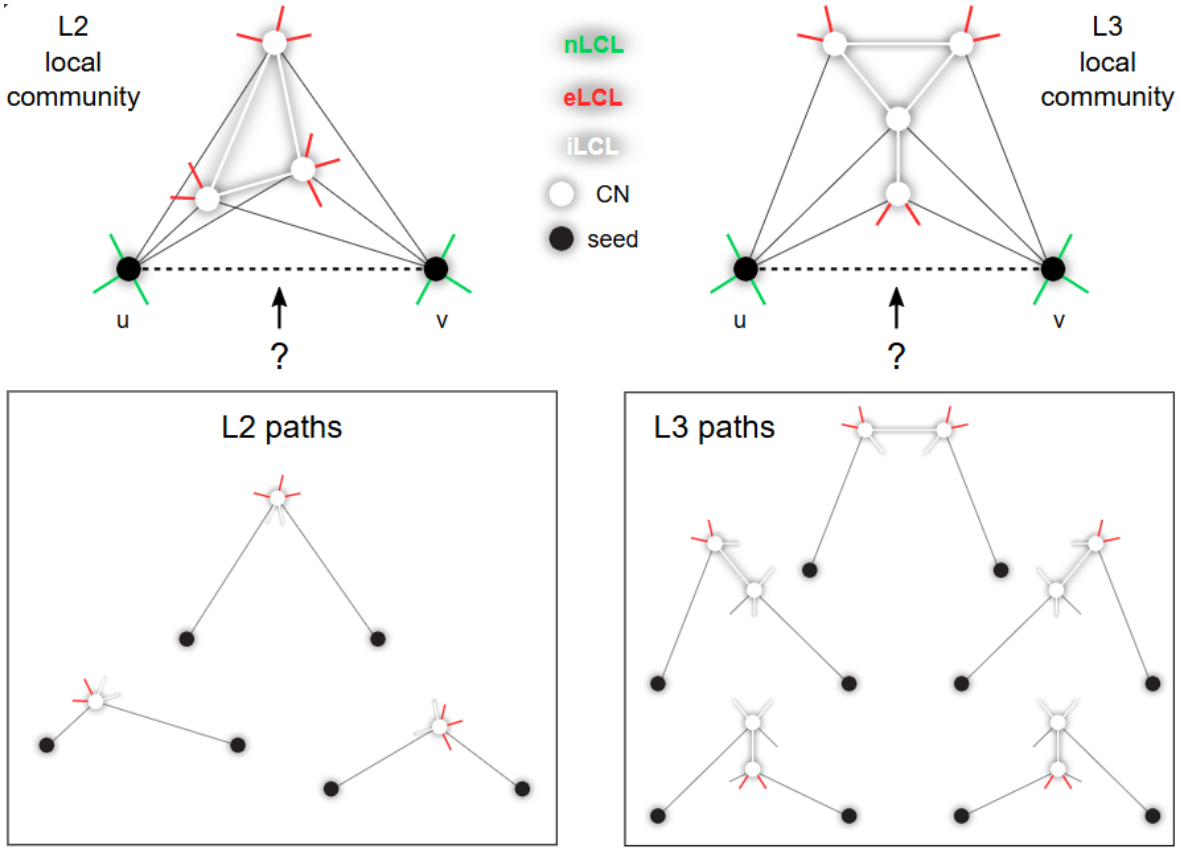

Model	*L2*	*L3*	*Ln*
RA	$\text{RA-L2}(u,v) = \sum_{z \in L_2} \frac{1}{d_z}$	$\text{RA-L3}(u,v) = \sum_{z_1,z_2 \in L_3} \frac{1}{\sqrt{d_{z_1} d_{z_2}}}$	$\text{RA-Ln}(u,v) = \sum_{z_1,\ldots,z_{n-1} \in L_n} \frac{1}{\left(\prod_{k=1}^{n-1} d_{z_k}\right)^{1/(n-1)}}$
CH1	$\text{CH1-L2}(u,v) = \sum_{z \in L_2} \frac{di_z}{d_z}$	$\text{CH1-L3}(u,v) = \sum_{z_1,z_2 \in L_3} \frac{\sqrt{di_{z_1} di_{z_2}}}{\sqrt{d_{z_1} d_{z_2}}}$	$\text{CH1-Ln}(u,v) = \sum_{z_1,\ldots,z_{n-1} \in L_n} \frac{\left(\prod_{k=1}^{n-1} di_{z_k}\right)^{1/(n-1)}}{\left(\prod_{k=1}^{n-1} d_{z_k}\right)^{1/(n-1)}}$
CH2	$\text{CH2-L2}(u,v) = \sum_{z \in L_2} \frac{di^*_z}{de^*_z}$	$\text{CH2-L3}(u,v) = \sum_{z_1,z_2 \in L_3} \frac{\sqrt{di^*_{z_1} di^*_{z_2}}}{\sqrt{de^*_{z_1} de^*_{z_2}}}$	$\text{CH2-Ln}(u,v) = \sum_{z_1,\ldots,z_{n-1} \in L_n} \frac{\left(\prod_{k=1}^{n-1} di^*_{z_k}\right)^{1/(n-1)}}{\left(\prod_{k=1}^{n-1} de^*_{z_k}\right)^{1/(n-1)}}$
CH3	$\text{CH3-L2}(u,v) = \sum_{z \in L_2} \frac{1}{de^*_z}$	$\text{CH3-L3}(u,v) = \sum_{z_1,z_2 \in L_3} \frac{1}{\sqrt{de^*_{z_1} de^*_{z_2}}}$	$\text{CH3-Ln}(u,v) = \sum_{z_1,\ldots,z_{n-1} \in L_n} \frac{1}{\left(\prod_{k=1}^{n-1} de^*_{z_k}\right)^{1/(n-1)}}$
CH3.1	$\text{CH3.1-L2}(u,v) = \sum_{z \in L_2} \frac{di^*_z}{de^{*\,1+de_z/de^*_z}_z}$	$\text{CH3.1-L3}(u,v) = \sum_{z_1,z_2 \in L_3} \frac{\sqrt{di^*_{z_1} di^*_{z_2}}}{\sqrt{de^{*\,1+de_{z_1}/de^*_{z_1}}_{z_1} de^{*\,1+de_{z_2}/de^*_{z_2}}_{z_2}}}$	$\text{CH3.1-Ln}(u,v) = \sum_{z_1,\ldots,z_{n-1} \in L_n} \frac{\left(\prod_{k=1}^{n-1} di^*_{z_k}\right)^{1/(n-1)}}{\left(\prod_{k=1}^{n-1} de^{*\,1+de_{z_k}/de^*_{z_k}}_{z_k}\right)^{1/(n-1)}}$

Figure A1. Cannistraci-Hebb epitopological rationale. The figure shows an explanatory example for the topological link prediction performed using the L2 or L3 Cannistraci-Hebb epitopological rationale. The two black nodes represent the seed nodes whose non-observed interaction should be scored with a likelihood. The white nodes are the L2 or L3 common-neighbours (CNs) of the seed nodes, further neighbours are not shown for simplicity. The cohort of common-neighbours and the iLCL form the local community. The different types of links are reported with different colours: non-LCL (green), external-LCL (red), internal-LCL (white). The set of L2 and L3 paths related to the given examples of local communities are shown. At the bottom, the mathematical description of the L2, L3 and Ln methods considered in this study are reported. Notation: u,v are the seed nodes; z is the intermediate node (CN) in the L2 path; d_z is the degree of z; di_z is the internal degree (number of iLCL) of z; de_z is the external degree (number of eLCL) of z. For any degree it is valid the following: $d^* = 1 + d$. For L3 and Ln paths the definitions are analogous.

 doi:10.20944/preprints202012.0808.v4

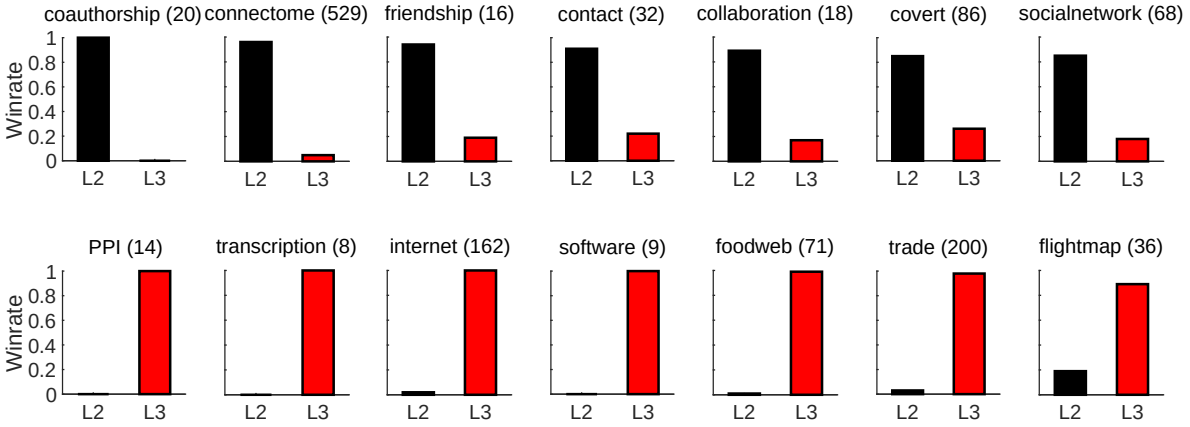

Figure A2. For each network of the ATLAS (considering $N \leq 10000$, 1269 networks) and for each CH model (RA, CH1, CH2, CH3, CH3.1) of path lengths L2-L3, we applied the 10% link removal evaluation, obtaining the AUPR as measure of performance . For each path length L2-L3, we assigned as performance on a network the maximum AUPR over the CH models. The barplots report for each network class and for each path length the win rate over the networks of that class. For each class, the number of networks is shown in brackets.

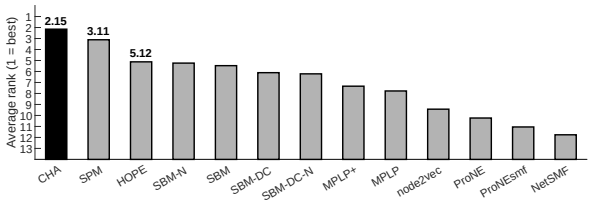

(**a**) ATLAS-small mean rank (NDCG)

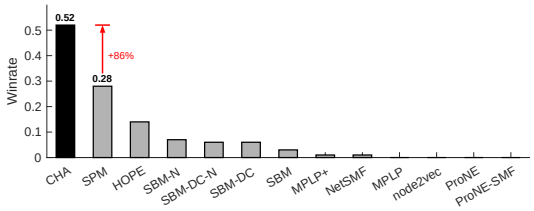

(**b**) ATLAS-small win rate (NDCG)

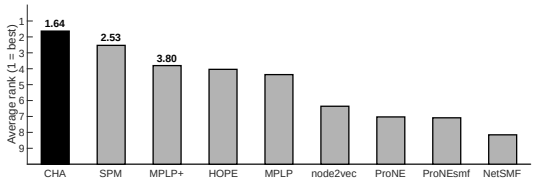

(**c**) ATLAS-medium mean rank (NDCG)

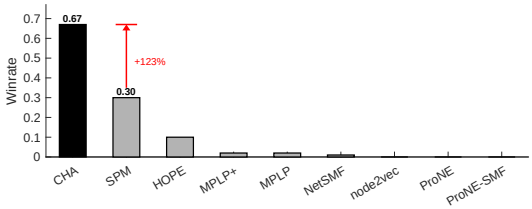

(**d**) ATLAS-medium win rate (NDCG)

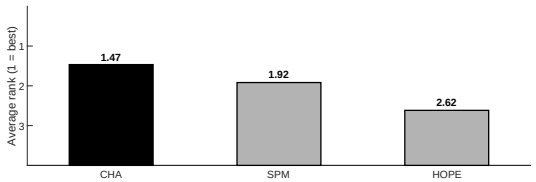

(**e**) ATLAS-large mean rank (NDCG)

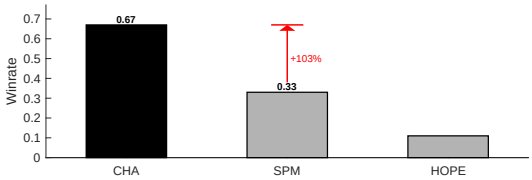

(**f**) ATLAS-large win rate (NDCG)

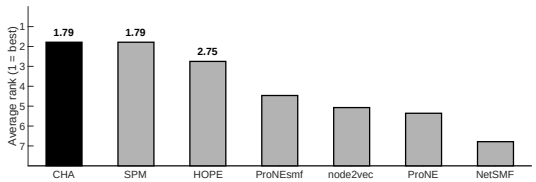

(**g**) ATLAS-temporal mean rank (NDCG)

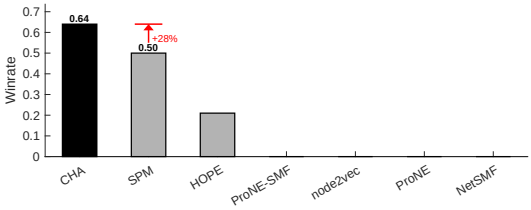

(**h**) ATLAS-temporal win rate (NDCG)

Figure A3. Comparison of CHA with baseline methods across network categories using NDCG.

 doi:10.20944/preprints202012.0808.v4

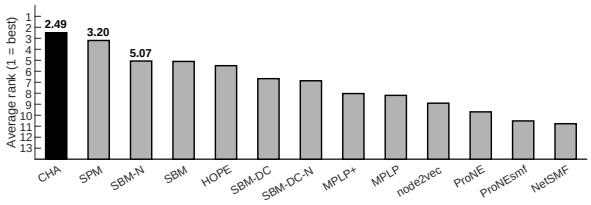

(**a**) ATLAS-small mean rank (Precision)

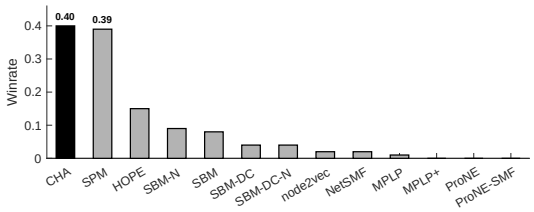

(**b**) ATLAS-small win rate (Precision)

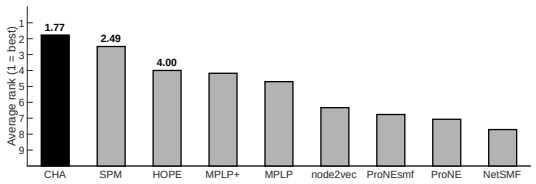

(**c**) ATLAS-medium mean rank (Precision)

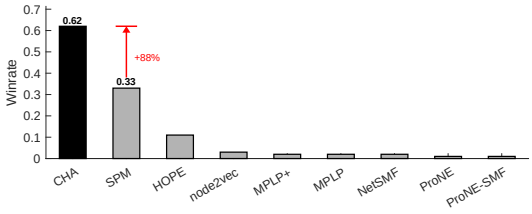

(**d**) ATLAS-medium win rate (Precision)

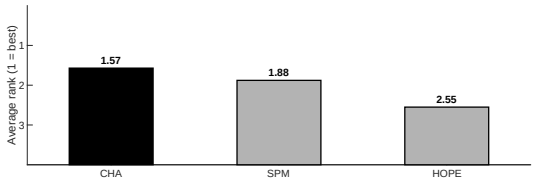

(**e**) ATLAS-large mean rank (Precision)

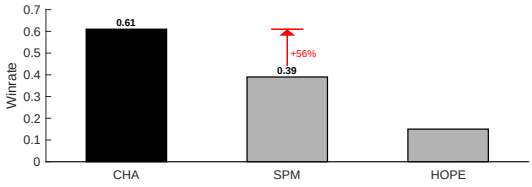

(**f**) ATLAS-large win rate (Precision)

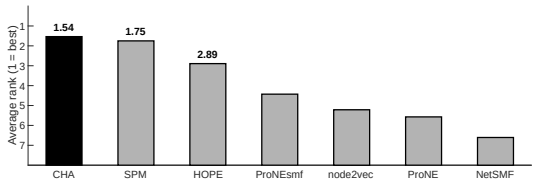

(**g**) ATLAS-temporal mean rank (Precision)

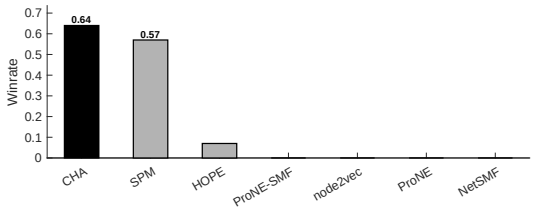

(**h**) ATLAS-temporal win rate (Precision)

Figure A4. Comparison of CHA with baseline methods across network categories using Precision.

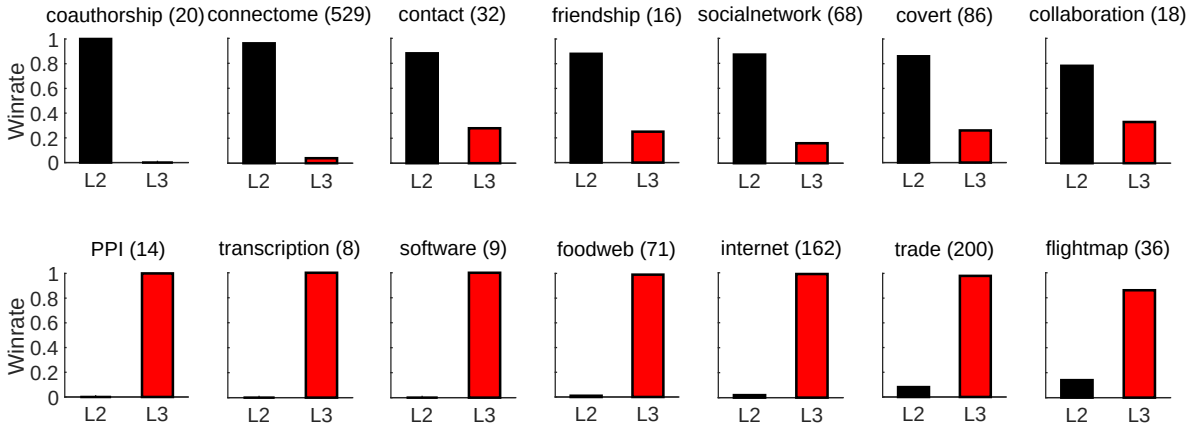

Figure A5. Path length preference across network classes based on Precision. For each network in ATLAS-static ($N \leq 10000$) and each CH model (RA, CH1, CH2, CH3, CH3.1), we compute Precision under 10% link removal. For each path length ($L2$, $L3$), we retain the best-performing CH model per network. Bar plots report the win rate of $L2$ versus $L3$ across networks in each class (class size in brackets).

 doi:10.20944/preprints202012.0808.v4

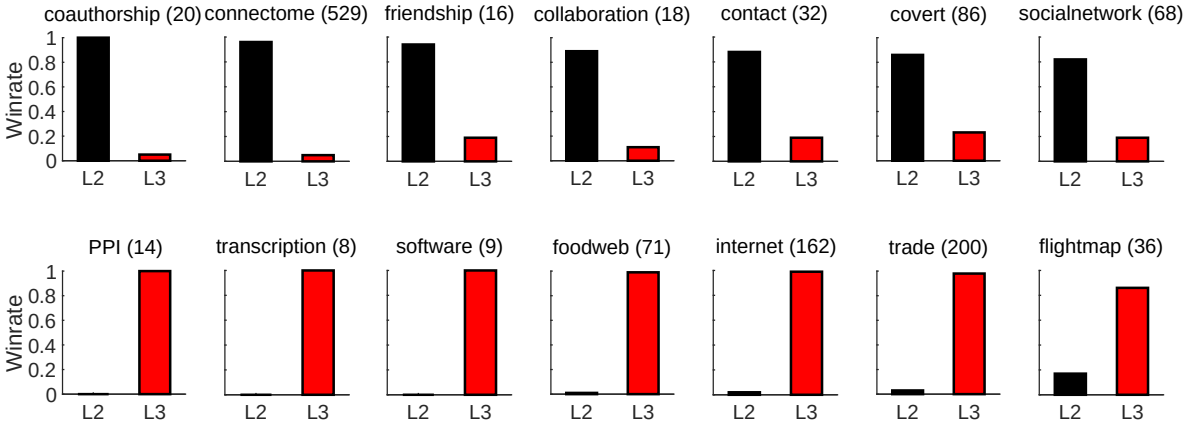

Figure A6. Path length preference across network classes based on NDCG. For each network in ATLAS-static ($N \leq 10000$) and each CH model (RA, CH1, CH2, CH3, CH3.1), we compute NDCG under 10% link removal. For each path length ($L2$, $L3$), we retain the best-performing CH model per network. Bar plots report the win rate of $L2$ versus $L3$ across networks in each class (class size in brackets).

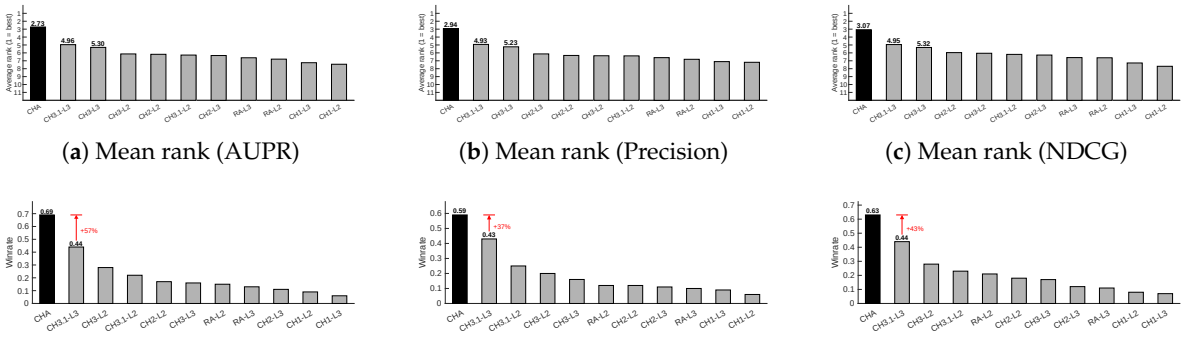

(**a**) Mean rank (AUPR) (**b**) Mean rank (Precision) (**c**) Mean rank (NDCG)

(**d**) Win rate (AUPR) (**e**) Win rate (Precision) (**f**) Win rate (NDCG)

Figure A7. Comparison of CHA and CH variants across evaluation metrics. For each network in ATLAS-static ($N \leq 10000$, 1269 networks), we apply the 10% link removal evaluation and compute both **mean rank** (top row) and **win rate** (bottom row) across three metrics: (a, d) AUPR, (b, e) Precision, and (c, f) NDCG. Bars report average values over the 14 network classes. In all cases, CHA achieves the best mean rank and highest win rate, consistently outperforming all individual CH variants.

 doi:10.20944/preprints202012.0808.v4

Table A1. Results of CHA variants on ATLAS-static. We evaluate several CHA variants on path lengths *L*2–*L*3, each using a different combination of CH models. For every network in ATLAS-static, we apply the 10% link removal evaluation and compute AUPR as the performance metric. For each network class, we report the **win rate** and **mean AUPR** of each algorithm across the networks in that class. The table shows the average of these values over all 14 classes. Algorithms are sorted by decreasing win rate. The upper bound indicates the performance that would be achieved by selecting the best CH model and path length per network.

Method	Win rate	AUPR
upper bound	1.00	0.30
CH3-CH3.1	0.72	0.29
CH2-CH3-CH3.1	0.72	0.29
RA-CH2-CH3-CH3.1	0.70	0.29
RA-CH3-CH3.1	0.69	0.29
CH2-CH3.1	0.67	0.28
CH3.1	0.65	0.28
RA-CH2-CH3.1	0.62	0.28
RA-CH3.1	0.60	0.28
CH1-CH3-CH3.1	0.56	0.27
CH1-CH2-CH3-CH3.1	0.56	0.27
CH1-CH2-CH3.1	0.54	0.26
RA-CH1-CH3-CH3.1	0.53	0.27
RA-CH1-CH2-CH3-CH3.1	0.53	0.27
CH1-CH3.1	0.52	0.26
RA-CH1-CH2-CH3.1	0.48	0.26
RA-CH1-CH3.1	0.47	0.26
CH3	0.41	0.28
CH2-CH3	0.41	0.28
RA-CH3	0.38	0.28
RA-CH2-CH3	0.38	0.28
CH2	0.26	0.27
RA-CH2	0.26	0.27
CH1-CH2-CH3	0.26	0.26
RA	0.25	0.26
CH1-CH3	0.25	0.26
RA-CH1-CH2-CH3	0.23	0.25
RA-CH1-CH3	0.22	0.25
CH1-CH2	0.16	0.25
RA-CH1-CH2	0.12	0.25
RA-CH1	0.12	0.24
CH1	0.10	0.23

Appendix B. Link Prediction Methods

Appendix B.1. Structural Perturbation Method (SPM)

The Structural Perturbation Method (SPM) is based on a theory analogous to the first-order perturbation technique in quantum mechanics [4]. A high-level description of the procedure is as follows:

1. Randomly remove 10% of the links from the network adjacency matrix X, obtaining a reduced network $X' = X - R$, where R is the set of removed links.
2. Compute the eigenvalues and eigenvectors of X'.
3. Considering the set of links R as a perturbation to X', construct the perturbed matrix X_P via a first-order approximation that allows the eigenvalues to change while keeping the eigenvectors fixed.
4. Repeat steps 1–3 for 10 independent iterations and take the average of the resulting perturbed matrices X_P.

 doi:10.20944/preprints202012.0808.v4

The link prediction result is given by the values in the averaged perturbed matrix, which represent the scores assigned to the non-observed links. A higher score indicates a higher likelihood that the corresponding interaction exists.

The rationale behind the method is that a missing portion of the network is predictable if its absence does not significantly alter the structural characteristics of the observable part, as captured by the eigenvectors of the adjacency matrix. If this condition holds, the perturbed matrices should serve as good approximations of the original network [4].

Appendix B.2. Stochastic Block Model (SBM)

The general idea behind the *Stochastic Block Model* (SBM) is that the nodes of a network are partitioned into B blocks, and a $B \times B$ matrix specifies the probabilities of links existing between nodes belonging to each pair of blocks. SBM provides a general framework for statistical analysis and inference in networks, particularly for tasks such as community detection and link prediction [37].

The concept of *degree-corrected* (DC) SBM was introduced for community detection [39] and for predicting spurious and missing links [38], in order to keep into account the variations in node degree typically observed in real networks. A *nested* (N) version of SBM has been introduced [5] to overcome two major limitations: the inability to separate true structures from noise, and the difficulty in detecting smaller yet well-defined clusters as network size increases.

All four tested variants (SBM, SBM-DC, SBM-N, SBM-DC-N) require finding an appropriate partitioning of the network to perform inference. We used the implementation provided in `Graph-tool` [40], which uses an optimized Markov Chain Monte Carlo (MCMC) algorithm to sample the space of possible partitions [37]. `Graph-tool` is a Python module available at: http://graph-tool.skewed.de/.

As suggested in [41], predictive performance is generally higher when averaging over multiple partitions rather than relying on a single most plausible partition, since the latter approach can lead to overfitting. Therefore, for each network, we sampled P partitions, computed the likelihood scores for the non-observed links in each partition, and averaged the scores across all partitions to obtain the final link prediction result. We set $P = 100$ for ATLAS networks with $N \leq 100$, and $P = 50$ for connectomes with $N > 100$.

Appendix B.3. HOPE

High-Order Proximity preserved Embedding (HOPE) is a graph embedding algorithm designed to preserve high-order proximities in graphs and to capture asymmetric transitivity [6]. Asymmetric transitivity depicts the correlation among directed edges, making HOPE particularly suitable for embedding directed networks, although it can also be used for undirected networks.

Many high-order proximity measures can reflect asymmetric transitivity in graphs, such as the *Katz index* [42]. Many of these measures share a common algebraic structure. Instead of computing the proximity matrix and then applying singular value decomposition (SVD), HOPE leverages this shared structure to transform the standard SVD problem into a *generalized SVD* problem. This formulation allows for the direct computation of embedding vectors, thereby avoiding explicit construction of the proximity matrix [6].

However, for the purpose of link prediction, an approximation of the proximity matrix can be reconstructed from the learned embedding. In this context, HOPE provides a scalable solution for approximating the Katz index through graph embedding. The entries of the approximated Katz proximity matrix represent the link prediction scores: the higher the proximity, the more likely the existence of the interaction.

The implementation of HOPE is available at: https://github.com/ZW-ZHANG/HOPE. For our experiments, we set the embedding dimension to $\min(128, N)$, where N is the number of nodes, and used the default values for all other parameters.

 doi:10.20944/preprints202012.0808.v4

Appendix B.4. node2vec

node2vec is a graph embedding algorithm that maps nodes to a low-dimensional feature space by maximizing the likelihood of preserving the network neighborhoods of nodes [7]. The maximization is performed on a custom graph-based objective function using stochastic gradient descent, inspired by prior work in natural language processing and related to the Skip-gram model [7].

To define node neighborhoods flexibly, node2vec employs a second-order random walk strategy to sample node neighborhoods. The behavior of the random walk is governed by two parameters: p (return parameter) and q (in-out parameter), which bias the walk towards different network exploration strategies (e.g., breadth-first vs. depth-first search).

After computing the node embeddings, we generate feature vectors for node pairs by applying the Hadamard (element-wise) product to the embedding vectors of each node in the pair, as suggested in the original node2vec study [7]. These node-pair feature vectors are then used to train a logistic regression classifier, which outputs likelihood scores for the non-observed links in the network.

The implementation of the node2vec embedding method is available at: https://github.com/snap-stanford/snap/. We set the embedding dimension to $\min(128, N-1)$, where N is the number of nodes, and discarded node features that were constant across all nodes.

We tested the parameters p and q using three configurations: $(p = 0.5, q = 2)$; $(p = 1, q = 1)$; and $(p = 2, q = 0.5)$. The best configuration was selected via cross-validation. All other parameters were kept at their default values.

Appendix B.5. ProNE and ProNE-SMF

ProNE has been proposed as a fast and scalable graph embedding algorithm that maps nodes to a low-dimensional feature space using a two-step procedure [9].

The first step initializes the network embedding using sparse matrix factorization (SMF), which efficiently provides an initial node representation via randomized truncated singular value decomposition. The second step, inspired by the higher-order Cheeger's inequality, performs *spectral propagation* to enhance the initial embedding [9].

In our analysis, we considered both the embeddings obtained after the first step (*ProNE-SMF*) and those obtained after the second step (*ProNE*).

After computing the embeddings, we generated feature vectors for node pairs by applying the Hadamard product to the corresponding node embeddings. These node-pair features were then used to train a logistic regression classifier to produce likelihood scores for the non-observed links in the network.

The implementation of the ProNE and ProNE-SMF embedding methods is available at: https://github.com/THUDM/ProNE/. We set the embedding dimension to $\min(128, N-1)$, where N is the number of nodes, and discarded node features that were constant across all nodes. Default values were used for all other parameters.

Appendix B.6. NetSMF

NetSMF is a graph embedding algorithm that maps nodes to a low-dimensional feature space [8]. It is based on the observation that several network embedding algorithms implicitly factorize a specific closed-form matrix, and that explicitly factorizing this matrix can lead to improved performance. However, the matrix in question is typically dense, making it computationally expensive to handle for large networks.

NetSMF addresses this limitation by proposing a scalable solution that first applies spectral graph sparsification techniques to construct a sparse matrix that is spectrally close to the original dense matrix. It then performs randomized singular value decomposition (SVD) on the sparse matrix to efficiently obtain the node embeddings [8].

 doi:10.20944/preprints202012.0808.v4

After generating the embeddings, we compute feature vectors for node pairs using the Hadamard product of their corresponding node embeddings. These pairwise feature vectors are then used to train a logistic regression classifier that produces likelihood scores for the non-observed links in the network.

The implementation of the NetSMF method is available at: https://github.com/xptree/NetSMF/. We set the embedding dimension to $\min(128, N-1)$, where N is the number of nodes, and discarded node features with constant values across all nodes. We set `rounds` = 10000 and used default values for all other parameters.

Appendix B.7. Logistic Regression Classifier

After obtaining feature vectors for each node pair from the network embeddings generated by *node2vec*, *ProNE*, *ProNE-SMF*, and *NetSMF*, we trained a logistic regression classifier to compute likelihood scores for the non-observed links in the network.

In particular, we performed a repeated 5-fold cross-validation 10 times. For each repetition $i \in [1, 10]$, the following steps were executed:

1. Create a learning set consisting of all the observed links and an equal number of non-observed links (if available; otherwise, include all non-observed links).
2. Split the learning set into 5 folds for cross-validation.
3. For each cross-validation iteration $j \in [1, 5]$:
   (a) *Train:* Train a logistic regression classifier using 4 folds and obtain the coefficient estimates $B_{i,j}$.
   (b) *Validation:* Using the coefficients $B_{i,j}$, obtain the likelihood scores for the remaining fold and compute the prediction performance using $\text{AUPR}_{i,j}$.

After completing the 10 repetitions, we compute the mean coefficient estimates $\bar{B}$ across all (i, j) pairs. These coefficients $\bar{B}$ are then used to compute the final likelihood scores for the non-observed links, which constitute the link prediction result.

In the case of *node2vec*, where multiple parameter configurations are tested, we also compute the mean validation performance $\overline{\text{AUPR}}$ over the 10 repetitions and 5 cross-validation iterations for each configuration. The final link prediction result corresponds to the configuration with the highest $\overline{\text{AUPR}}$.

In contrast, for *ProNE*, *ProNE-SMF*, and *NetSMF*, which use a single parameter configuration, step 3.(b) (validation) is not necessary.

We used the MATLAB implementation of the logistic regression classifier, specifically the `mnrfit` and `mnrval` functions, to perform model training and scoring.

Appendix B.8. MPLP and MPLP+

Message Passing Link Predictor (MPLP) is a graph neural model specifically designed for the link prediction task [10]. Unlike general-purpose graph embedding methods that focus on node-level representations, MPLP explicitly estimates link-level structural features such as the Common Neighbor (CN) score. It achieves this by propagating quasi-orthogonal vectors through message-passing layers and leveraging their inner products to approximate structural similarities between node pairs.

To improve scalability, *MPLP+* introduces a more efficient variant that avoids expensive multi-hop preprocessing. Instead, it computes approximated structural signals using only one-hop neighborhoods, making it suitable for large-scale graphs with limited memory or time constraints.

The official implementation is available at: https://github.com/Barcavin/efficient-node-labelling. In this study, we followed the original MPLP experimental settings, with the exception of the early stopping strategy. The original implementation used Hits@100 on a validation set with a 1:1 positive-to-negative ratio, which is not consistent with our evaluation metric, AUPR, where positives are ranked among all missing links. This misalignment could result in suboptimal model selection. To address this, we modified MPLP's early stopping criterion to monitor the AUPR on the validation set and stop training when it no longer improves, ensuring better alignment with our evaluation framework.

 doi:10.20944/preprints202012.0808.v4

Appendix C. Link Prediction Evaluation

Appendix C.1. 10% Link Removal Evaluation

The 10% link removal evaluation framework is employed when there is no information available about missing links or links that may appear in the future relative to the current state of the network.

Given a network X, 10% of its links are randomly removed, resulting in a reduced network $X' = X - R$, where R is the set of removed links. To evaluate a given algorithm, the reduced network X' is provided as input, and the algorithm outputs likelihood scores for the non-observed links in X'.

These non-observed links are ranked in descending order of their predicted scores. The removed links R are treated as positives, and the remaining non-links as negatives. Evaluation metrics such as area under the precision-recall curve (AUPR), Precision, and normalized discounted cumulative gain (NDCG) are computed to assess the ranking quality.

Because the link removal is random, the procedure is repeated 10 times with different train/test splits. The final performance on network X is reported as the average metric over these repetitions.

Appendix C.2. Temporal Evaluation

The temporal evaluation framework is employed when information is available regarding links that will appear in the future relative to the current time point of the network under consideration.

For a given network, a sequence of T snapshots is available, each corresponding to a different time point. For each snapshot at time $i \in [1, T-1]$, the snapshot is provided as input to the algorithm being evaluated, which outputs likelihood scores for the non-observed links at time i.

For each pair of time points (i, j) with $i \in [1, T-1]$ and $j \in [i+1, T]$, the non-observed links at time i are ranked by their predicted scores, and the links that actually appear at time j are treated as positives. Non-observed links at time i involving nodes that no longer exist at time j are excluded from the evaluation.

Multiple ranking-based metrics are computed for each (i, j) pair, including area under the precision-recall curve (AUPR), Precision, and normalized discounted cumulative gain (NDCG). The final performance for the network is reported as the average of each metric over all valid time pairs.

Appendix D. Datasets

Appendix D.1. ATLAS

We have collected a dataset of 1269 real-world networks, either downloaded from publicly available online sources or provided directly by the authors of prior scientific studies. The networks have been categorized into 14 distinct classes, with the number of networks in each class

Table A2. Number of networks per class.

Class	Count
Collaboration	18
Contact	32
Covert	86
Friendship	16
PPI	14
Connectome	529
Foodweb	71
Trade	200
Transcription	8
Coauthorship	20
Flightmap	36
Internet	162
Socialnetwork	68
Software	9
Total	**1269**

 doi:10.20944/preprints202012.0808.v4

For a complete list of the networks along with their basic properties (such as number of nodes and edges), references, data sources, and descriptions, please refer to Supplementary Material.

Appendix D.2. Temporal Networks

We have collected a dataset of 14 real networks with temporal information, downloaded from publicly available online sources. For each network, a certain number of snapshots are available, corresponding to different time points.

For a complete list of the networks along with their basic properties (such as number of nodes and edges), references, data sources, and descriptions, please refer to Supplementary Material.

Appendix E. Compute Resources

All experiments were conducted on a high-performance computing server equipped with 256 logical CPUs and 2 TB of RAM. The machine supports 64-bit architecture with 256 MiB of L3 cache and a base frequency of 1.5 GHz (boost up to 2.6 GHz). No GPUs were used, as CHA is CPU-based.

We estimate that running all 1269 networks required approximately 72 CPU hours.

Appendix F. Time Complexity and Runtime Analysis

Appendix F.1. Time Complexity of CHA

The time complexity of CHA is determined by the number of length-ℓ paths in the network and the cost of computing iLCL and eLCL statistics for the intermediate nodes along those paths.

Let n and m denote the number of nodes and edges, respectively. $\bar{d} = 2m/n$ is the average degree.

Appendix F.1.1. For $\ell = 2$.

- **Path count.** Each length-2 path $u \to z \to v$ is defined by an intermediate node z connected to both u and v. The total number of such paths is given by:

$$\#\text{L2\_path} = \sum_{z=1}^{n} \binom{d_z}{2} = \sum_{z=1}^{n} \frac{d_z(d_z-1)}{2} = \mathcal{O}\left(\sum_{z=1}^{n} d_z^2\right)$$

  where d_z is the degree of node z. This represents the number of unique unordered two-hop paths in the network.
- **Computation per path.** For each length-2 path, CHA computes a score based on the iLCL and eLCL of the intermediate node z. This requires checking the neighbors of z against the local community associated with the pair (u, v), which takes $\mathcal{O}(d_z)$ time per path.
- **Overall time complexity.** Multiplying the path count and per-path cost gives the total time complexity:

$$\mathcal{O}\left(\sum_{z=1}^{n} d_z^2 \cdot d_z\right) = \mathcal{O}\left(\sum_{z=1}^{n} d_z^3\right)$$

  We now analyze this quantity under three typical network regimes:
- *Sparse, degree-homogeneous:* If the graph is Sparse (i.e. $\bar{d} = 2m/n = \mathcal{O}(1)$) with relatively uniform degrees (i.e., $d_z = \mathcal{O}(1)$ for all z), then:

$$\mathcal{O}\left(\sum_{z=1}^{n} d_z^3\right) = \mathcal{O}(n)$$

  So the overall time complexity of $\mathcal{O}(n)$.
- *Sparse, degree-heterogeneous:* If the graph is sparse (i.e., $\bar{d} = \mathcal{O}(1)$), but has a skewed degree distribution (e.g., power law), we can no longer assume $d_z = \mathcal{O}(1)$ for all nodes. To handle

 doi:10.20944/preprints202012.0808.v4

this case, we apply a relaxation via Hölder's inequality [43] to upper-bound the root-mean-cube degree $\left(\frac{1}{n}\sum_z d_z^3\right)^{1/3}$ in terms of the average degree:

$$\left(\frac{1}{n}\sum_{z=1}^{n} d_z^3\right)^{1/3} \le n^{2/3}\cdot\left(\frac{1}{n}\sum_{z=1}^{n} d_z\right) = n^{2/3}\cdot\bar{d} = \mathcal{O}(n^{2/3})$$

This relaxation allows us to express the cubic-degree term in the overall complexity as:

$$\mathcal{O}\left(\sum_{z=1}^{n} d_z^3\right) = \mathcal{O}\left(n\cdot\left(\frac{1}{n}\sum_{z=1}^{n} d_z^3\right)\right) = \mathcal{O}\left(n\cdot\left(n^{2/3}\right)^3\right) = \mathcal{O}(n^3)$$

Thus, the overall time complexity in this case is $\mathcal{O}(n^3)$.

- *Dense graphs:* In the worst-case scenario of dense graphs, where $d_z = \mathcal{O}(n)$ for all nodes, we obtain:

$$\sum_{z=1}^{n} d_z^3 = \mathcal{O}(n^4)$$

leading to an overall time complexity of $\mathcal{O}(n^4)$.

Appendix F.1.2. For $\ell = 3$

- **Path count.** Each length-3 path $u \to i \to j \to v$ passes through a central edge $(i,j) \in E$. The number of such paths using (i,j) as the central segment is $(d_i - 1)(d_j - 1)$, where d_i and d_j are the degrees of i and j, respectively. The total number of such paths is:

$$\#\text{L3\_path} = \sum_{(i,j)\in E}(d_i - 1)(d_j - 1) = \mathcal{O}\left(\sum_{(i,j)\in E} d_i d_j\right)$$

- **Computation per path.** For each length-3 path $u \to i \to j \to v$, CHA computes the iLCL and eLCL of intermediate nodes i and j with respect to the seed pair (u,v).
Each such computation, i.e., evaluating the iLCL/eLCL of node i with respect to (u,v), requires scanning the neighborhood of i and takes $\mathcal{O}(d_i)$ time. However, this computation is performed only once for each triplet (u,v,i), and the result is reused across all paths in which (u,v,i) appears. Since each such triplet (u,v,i) is associated with $\mathcal{O}(d_i)$ paths on average, the total cost is distributed across multiple paths. Thus, the amortized cost per path remains $\mathcal{O}(1)$.
- **Overall time complexity.** For compact notation, we define the RMS degree–degree product over edges:

$$\tilde{d}_{\text{edge}} = \sqrt{\frac{1}{m}\sum_{(i,j)\in E} d_i d_j}$$

and upper bound the total complexity as:

$$\mathcal{O}\left(m\cdot\tilde{d}_{\text{edge}}^2\right)$$

We now analyze this quantity under three typical network regimes:

- *Sparse, degree-homogeneous:* If the graph is sparse (i.e., $\bar{d} = \mathcal{O}(1)$) with relatively uniform degrees (i.e., $d_i = \mathcal{O}(1)$ for all nodes), then $d_i d_j = \mathcal{O}(1)$ for all edges and $m = \mathcal{O}(n)$. This yields:

$$\mathcal{O}\left(m\cdot\tilde{d}_{\text{edge}}^2\right) = \mathcal{O}(n)$$

So the overall time complexity of $\mathcal{O}(n)$.

 doi:10.20944/preprints202012.0808.v4

- *Sparse, degree-heterogeneous:* If the graph is sparse (i.e., $\bar{d} = \mathcal{O}(1)$), but has a skewed degree distribution (e.g., power law), we upper bound:

$$\tilde{d}^2_{\text{edge}} = \frac{1}{m} \sum_{(i,j)\in E} d_i d_j \leq \max_{(i,j)} d_i d_j$$

  In the worst case, this maximum can scale as $\mathcal{O}(n^2)$. Since the total number of edges is $m = \frac{n\cdot\bar{d}}{2}$, it follows that $m = \mathcal{O}(n)$. This leads to an overall complexity:

$$\mathcal{O}(m \cdot \tilde{d}^2_{\text{edge}}) = \mathcal{O}(n \cdot n^2) = \mathcal{O}(n^3)$$

- *Dense networks:* If the network is dense ($m = \mathcal{O}(n^2)$ and degrees are $\mathcal{O}(n)$), then $\tilde{d}_{\text{edge}} = \mathcal{O}(n)$ and:

$$\mathcal{O}(m \cdot \tilde{d}^2_{\text{edge}}) = \mathcal{O}(n^4)$$

Appendix F.1.3. Summary

The overall time complexity of CHA depends on the path length ℓ (only when $l \geq 4$) and the structural characteristics of the network. For both $\ell = 2$ and $\ell = 3$, we observe the following regimes:

- *Sparse, degree-homogeneous:* When the average degree is $\mathcal{O}(1)$ and degree distribution is uniform, the complexity is: $\mathcal{O}(n)$
- *Sparse, degree-heterogeneous:* When the average degree is $\mathcal{O}(1)$ but degree distribution is skewed (e.g., power-law), the complexity is higher due to hubs: $\mathcal{O}(n^3)$
- *Dense networks:* When the average degree is $\mathcal{O}(n)$, the worst-case complexity becomes $\mathcal{O}(n^4)$

Although CHA internally evaluates multiple CH models and path lengths, all models operate on the same set of intermediate-node statistics (iLCL and eLCL), which are computed only once. Therefore, evaluating multiple models does not increase the overall asymptotic complexity.

Appendix F.1.4. Subranking Complexity

The subranking step based on Spearman correlation requires computing all-pairs shortest paths, which has a worst-case time complexity of $\mathcal{O}(n^3)$.

Appendix F.2. Running Time of CHA

We empirically evaluate the running time of CHA under different graph conditions to validate its efficiency in practice.

Figure A8 reports the average edge density across networks of increasing size in the ATLAS-static dataset. While the overall dataset has moderately low density (0.1946), the average density for larger networks ($N > 2500$) drops sharply to 0.0058. This confirms that large real-world networks in ATLAS are typically sparse.

To further explore CHA's computational behavior under varying sparsity levels, Figure A9 shows its running time on synthetic networks with 500 nodes and increasing edge densities. The edge density is defined as the average degree divided by $N - 1$. As predicted by theoretical analysis, computation time increases steeply with density. For sparse graphs, CHA is significantly faster.

Together, these results indicate that CHA benefits from the inherent sparsity of real-world networks and achieves high scalability across the ATLAS benchmark.

 doi:10.20944/preprints202012.0808.v4

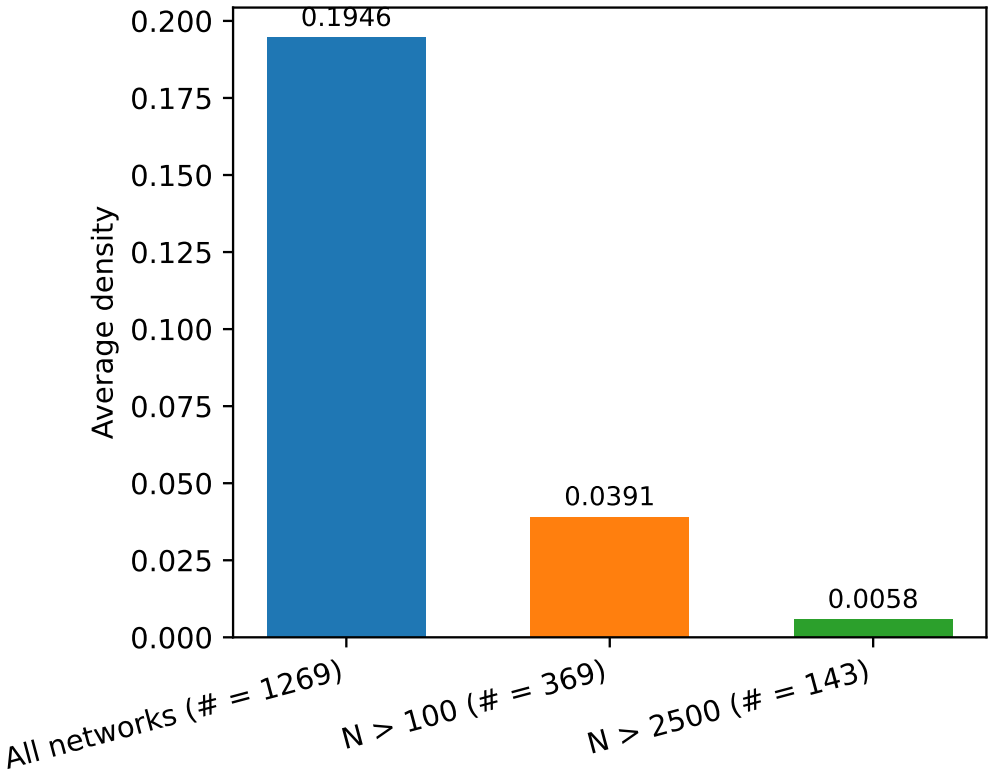

Figure A8. Average edge density across different network sizes in ATLAS-static. We report the average edge density, defined as the ratio between average degree and $N-1$, for three subsets of the ATLAS-static dataset: all networks ($N = 1269$, density = 0.1946), networks with $N > 100$ ($n = 369$, density = 0.0391), and networks with $N > 2500$ ($n = 143$, density = 0.0058). The results show that large networks in ATLAS-static are extremely sparse, which makes CHA extremely fast to compute on such networks. (see Figure A9).

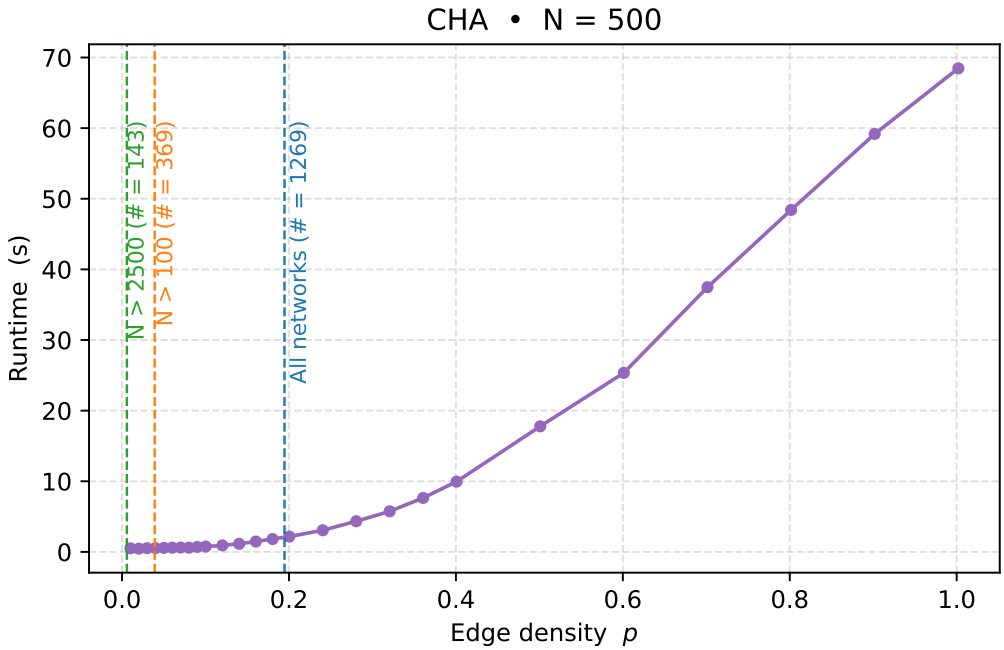

Figure A9. Runtime of CHA on artificial networks with increasing density. We generate synthetic networks with $N = 500$ nodes and vary the density, defined as average degree divided by $(N-1)$. The plot shows that CHA runs extremely fast on sparse networks, while its runtime increases rapidly as density grows. This highlights the efficiency of CHA in low-density regimes, which are common in many real-world networks.

 doi:10.20944/preprints202012.0808.v4

Appendix G. Mapping Subranking to Likelihood Score

The CH sub-ranking mechanism refines the ordering of node pairs with tied CH scores by leveraging secondary scores (e.g., SPcorr). In some applications, it is desirable to map this refined ranking back to continuous likelihood scores.

To achieve this, we provide two interpolation-based strategies that preserve the original CH ranking while assigning distinct values to previously tied scores:

- **Score-guided interpolation.** Tied scores are adjusted based on the actual SPcorr values, preserving their relative magnitudes within the group. This results in a smooth, value-aware distribution of scores.
- **Rank-based interpolation.** Tied scores are redistributed uniformly according to their sub-rank positions, regardless of the SPcorr values. This maintains only the order but not the magnitude.

Both strategies are optional and not used during the main CHA evaluation, but are supported for downstream scenarios requiring continuous-valued outputs.

References

1. Lü, L.; Zhou, T. Link prediction in complex networks: A survey. *Physica A: statistical mechanics and its applications* **2011**, *390*, 1150–1170.
2. Liben-Nowell, D.; Kleinberg, J. The link prediction problem for social networks. In Proceedings of the Proceedings of the twelfth international conference on Information and knowledge management, 2003, pp. 556–559.
3. Cannistraci, C.V.; Alanis-Lobato, G.; Ravasi, T. From link-prediction in brain connectomes and protein interactomes to the local-community-paradigm in complex networks. *Scientific reports* **2013**, *3*, 1613.
4. Lü, L.; Pan, L.; Zhou, T.; Zhang, Y.C.; Stanley, H.E. Toward link predictability of complex networks. *Proceedings of the National Academy of Sciences* **2015**, *112*, 2325–2330.
5. Peixoto, T.P. Hierarchical block structures and high-resolution model selection in large networks. *Physical Review X* **2014**, *4*, 011047.
6. Ou, M.; Cui, P.; Pei, J.; Zhang, Z.; Zhu, W. Asymmetric transitivity preserving graph embedding. In Proceedings of the Proceedings of the 22nd ACM SIGKDD international conference on Knowledge discovery and data mining, 2016, pp. 1105–1114.
7. Grover, A.; Leskovec, J. node2vec: Scalable feature learning for networks. In Proceedings of the Proceedings of the 22nd ACM SIGKDD international conference on Knowledge discovery and data mining, 2016, pp. 855–864.
8. Qiu, J.; Dong, Y.; Ma, H.; Li, J.; Wang, C.; Wang, K.; Tang, J. NetSMF: Large-scale network embedding as sparse matrix factorization. In Proceedings of the The World Wide Web Conference, 2019, pp. 1509–1520.
9. Zhang, J.; Dong, Y.; Wang, Y.; Tang, J.; Ding, M. Prone: Fast and scalable network representation learning. In Proceedings of the IJCAI, 2019, Vol. 19, pp. 4278–4284.
10. Dong, K.; Guo, Z.; Chawla, N. Pure message passing can estimate common neighbor for link prediction. *Advances in Neural Information Processing Systems* **2024**, *37*, 73000–73035.
11. Daminelli, S.; Thomas, J.M.; Durán, C.; Cannistraci, C.V. Common neighbours and the local-community-paradigm for topological link prediction in bipartite networks. *New Journal of Physics* **2015**, *17*, 113037.
12. Durán, C.; Daminelli, S.; Thomas, J.M.; Haupt, V.J.; Schroeder, M.; Cannistraci, C.V. Pioneering topological methods for network-based drug–target prediction by exploiting a brain-network self-organization theory. *Briefings in bioinformatics* **2018**, *19*, 1183–1202.
13. Cannistraci, C.V. Modelling self-organization in complex networks via a brain-inspired network automata theory improves link reliability in protein interactomes. *Scientific Reports* **2018**, *8*, 15760.
14. Muscoloni, A.; Michieli, U.; Cannistraci, C.V. Local-ring network automata and the impact of hyperbolic geometry in complex network link-prediction. *arXiv preprint arXiv:1707.09496* **2017**.
15. Muscoloni, A.; Abdelhamid, I.; Cannistraci, C.V. Local-community network automata modelling based on length-three-paths for prediction of complex network structures in protein interactomes, food webs and more. *BioRxiv* **2018**, p. 346916.

 doi:10.20944/preprints202012.0808.v4

16. Zhou, T.; Lee, Y.L.; Wang, G. Experimental analyses on 2-hop-based and 3-hop-based link prediction algorithms. *Physica A: Statistical Mechanics and its Applications* **2021**, *564*, 125532.
17. Newman, M.E. Clustering and preferential attachment in growing networks. *Physical review E* **2001**, *64*, 025102.
18. Zhou, T.; Lü, L.; Zhang, Y.C. Predicting missing links via local information. *The European Physical Journal B* **2009**, *71*, 623–630.
19. Jaccard, P. Distribution comparée de la flore alpine dans quelques régions des Alpes occidentales et orientales. *Bulletin de la Murithienne* **1902**, pp. 81–92.
20. Kovács, I.A.; Luck, K.; Spirohn, K.; Wang, Y.; Pollis, C.; Schlabach, S.; Bian, W.; Kim, D.K.; Kishore, N.; Hao, T.; et al. Network-based prediction of protein interactions. *Nature communications* **2019**, *10*, 1240.
21. Barabási, A.L.; Albert, R. Emergence of Scaling in Random Networks. *Science* **1999**, *286*, 509–512, [https://www.science.org/doi/pdf/10.1126/science.286.5439.509]. https://doi.org/10.1126/science.286.5439.509.
22. Papadopoulos, F.; Kitsak, M.; Serrano, M.Á.; Boguñá, M.; Krioukov, D. Popularity versus similarity in growing networks. *Nature* **2012**, *489*, 537–540. https://doi.org/10.1038/nature11459.
23. Muscoloni, A.; Cannistraci, C.V. A nonuniform popularity-similarity optimization (nPSO) model to efficiently generate realistic complex networks with communities. *New Journal of Physics* **2018**, *20*, 052002. https://doi.org/10.1088/1367-2630/aac06f.
24. Wolfram, S.; Gad-el Hak, M. A new kind of science. *Appl. Mech. Rev.* **2003**, *56*, B18–B19.
25. Smith, D.M.; Onnela, J.P.; Lee, C.F.; Fricker, M.D.; Johnson, N.F. Network automata: Coupling structure and function in dynamic networks. *Advances in Complex Systems* **2011**, *14*, 317–339.
26. Marr, C.; Hütt, M.T. Topology regulates pattern formation capacity of binary cellular automata on graphs. *Physica A: Statistical Mechanics and its Applications* **2005**, *354*, 641–662.
27. Hebb, D. The Organization of Behavior. emphNew York, 1949.
28. Liu, Z.; He, J.L.; Kapoor, K.; Srivastava, J. Correlations between community structure and link formation in complex networks. *PloS one* **2013**, *8*, e72908.
29. Pan, L.; Zhou, T.; Lü, L.; Hu, C.K. Predicting missing links and identifying spurious links via likelihood analysis. *Scientific reports* **2016**, *6*, 22955.
30. Tan, F.; Xia, Y.; Zhu, B. Link prediction in complex networks: a mutual information perspective. *PloS one* **2014**, *9*, e107056.
31. Wang, W.; Cai, F.; Jiao, P.; Pan, L. A perturbation-based framework for link prediction via non-negative matrix factorization. *Scientific reports* **2016**, *6*, 38938.
32. Wang, T.; Wang, H.; Wang, X. CD-Based indices for link prediction in complex network. *Plos one* **2016**, *11*, e0146727.
33. Pech, R.; Hao, D.; Pan, L.; Cheng, H.; Zhou, T. Link prediction via matrix completion. *Europhysics Letters* **2017**, *117*, 38002.
34. Shakibian, H.; Moghadam Charkari, N. Mutual information model for link prediction in heterogeneous complex networks. *Scientific reports* **2017**, *7*, 44981.
35. Narula, V.; Zippo, A.G.; Muscoloni, A.; Biella, G.E.M.; Cannistraci, C.V. Can local-community-paradigm and epitopological learning enhance our understanding of how local brain connectivity is able to process, learn and memorize chronic pain? *Applied Network Science* **2017**, *2*, 1–28.
36. Rees, C.L.; Moradi, K.; Ascoli, G.A. Weighing the evidence in Peters' rule: does neuronal morphology predict connectivity? *Trends in neurosciences* **2017**, *40*, 63–71.
37. Peixoto, T.P. Efficient Monte Carlo and greedy heuristic for the inference of stochastic block models. *Physical Review E* **2014**, *89*, 012804.
38. Zhang, X.; Wang, X.; Zhao, C.; Yi, D.; Xie, Z. Degree-corrected stochastic block models and reliability in networks. *Physica A: Statistical Mechanics and its Applications* **2014**, *393*, 553–559.
39. Karrer, B.; Newman, M.E. Stochastic blockmodels and community structure in networks. *Physical Review E—Statistical, Nonlinear, and Soft Matter Physics* **2011**, *83*, 016107.
40. Peixoto, T.P. The Graph-tool Python Library. https://doi.org/10.6084/m9.figshare.1164194, 2014. https://doi.org/10.6084/m9.figshare.1164194.
41. Vallès-Català, T.; Peixoto, T.P.; Sales-Pardo, M.; Guimerà, R. Consistencies and inconsistencies between model selection and link prediction in networks. *Physical Review E* **2018**, *97*, 062316.

 doi:10.20944/preprints202012.0808.v4

42. Katz, L. A new status index derived from sociometric analysis. *Psychometrika* **1953**, *18*, 39–43.
43. Stein, E.M.; Shakarchi, R. *Real Analysis: Measure Theory, Integration, and Hilbert Spaces*; Princeton University Press, 2005.